East European Journal of Physics. 3. 251-268 (2026)
DOI:10.26565/2312-4334-2026-3-20 ISSN 2312-4334

GOLD-INDUCED MAGNETISM AND THERMAL STABILITY IN SiC NANOSHEETS: DFT+U

Sevda Rzayeva[1]*, Yuldosh Yakubov[2], Umedjon Khalilov[3,4,5], Maftun Aliyev[6], Ariel Sharon Asare[7,8]
[1]*Azerbaijan State Oil and Industry University, 20 Azadlig Ave., AZ-1010, Baku, Azerbaijan*
[2]*Institute of General and Inorganic Chemistry, Mirzo-Ulugbek 77-a, 100170 Tashkent, Uzbekistan*
[3]*Arifov Institute of Ion-Plasma and Laser Technologies, Durmon yuli 33, 100120 Tashkent, Uzbekistan*
[4]*University of Antwerp, Groenenborgerlaan 171, Antwerp 2020, Belgium*
[5]*Engineering School, Central Asian University, Tashkent 111221, Uzbekistan*
[6]*Nakhchivan State University, Nakhchivan, Azerbaijan*
[7]*Department of Physics, University of Ghana*
[8]*Abdus Salam International Centre for Theoretical Physics (ICTP), Italy*
**Corresponding author: rzayeva.sevda@asoiu.edu.az*
Received April 12, 2026; revised June 21, 2026; accepted July 2, 2026

Gold-doped two-dimensional silicon carbide (SiC) nanosheets are investigated using spin-polarized density functional theory (DFT+U) to examine their electronic structure, induced magnetism, and thermal stability. Single (1Au@Si) and double (2Au@2Si) substitutional configurations are modeled within a 4×4 supercell to ensure reliable evaluation of intrinsic properties. Au incorporation significantly narrows the band gap while preserving the semiconducting character of the SiC nanosheet. Spin-resolved density-of-states analysis shows that Au 5d orbitals dominate the electronic states near the Fermi level. Despite nearly spin-degenerate band dispersions, Mulliken spin population analysis reveals dopant-induced magnetism mediated by neighboring carbon atoms. The 1Au@Si system exhibits a magnetic moment of ~3 μ_B, while the 2Au@2Si configuration stabilizes a ferrimagnetic-like state with a total magnetic moment of ~6 μB. Within the mean-field approximation, the estimated Curie temperature is approximately 510 K, suggesting the possibility of magnetic stability above room temperature and potential applications in spintronic devices.
Keywords: *SiC nanosheets; Gold doping; Spintronics; Dilute magnetic semiconductors; Density functional theory; Curie temperature*

1. INTRODUCTION

Two-dimensional (2D) materials have emerged as one of the most compelling platforms for investigating spin-dependent phenomena at the nanoscale. Owing to strong quantum confinement effects and reduced dielectric screening, the electronic states in 2D systems exhibit exceptional sensitivity to external perturbations such as elemental doping, intrinsic defects, and applied strain [1-3]. This heightened responsiveness enables precise atomic-scale control over charge, spin, and magnetic degrees of freedom, positioning 2D materials at the forefront of next-generation spintronic and nano-electronic technologies.

Within this rapidly expanding research field, two-dimensional silicon carbide (SiC) nanosheets have attracted increasing attention as wide-band-gap semiconductors due to their exceptional thermal stability, chemical inertness, high mechanical robustness, and strong resistance to radiation-induced degradation [4,5]. Unlike many conventional 2D materials, SiC nanosheets retain their structural integrity and electronic characteristics under extreme environmental and operating conditions, making them particularly attractive for high-performance and durable device applications.

Despite these favorable properties, pristine SiC nanosheets are intrinsically non-magnetic and have relatively wide band gaps, which severely limit their direct applicability to spintronic devices that require finite spin polarization and stable long-range magnetic ordering. To overcome this intrinsic limitation, substitutional doping has been widely employed as an effective strategy, as it can induce pronounced electronic reconstruction and generate spin polarization through strong dopant–host orbital hybridization [6,7].

Although considerable research efforts have been devoted to transition-metal (3d) doping in SiC-based nanostructures, such dopants often induce strong electronic localization, clustering tendencies, or undesirable metallic behavior. These effects can adversely influence carrier mobility, magnetic stability, and overall device performance, thereby limiting their practical applicability [8-13].

In contrast, noble-metal dopants-particularly gold (Au)-offer an alternative and fundamentally distinct route for engineering the electronic and magnetic properties of low-dimensional systems. Gold is characterized by spatially extended 5d orbitals, pronounced relativistic effects, and strong spin–orbit coupling, which collectively enable substantial modification of the host electronic structure without necessarily inducing a semiconductor-to-metal transition [9, 14, 15]. Recent theoretical studies suggest that substitutional Au incorporation can introduce impurity-derived states near the band edges and promote strong hybridization with host p orbitals. Nevertheless, the microscopic origin of magnetism in Au-doped SiC nanosheets remains insufficiently understood. In particular, it is still unclear whether the induced magnetic moments are primarily localized on the Au dopants or are mediated through the surrounding Si-C lattice, with a potentially dominant contribution arising from the carbon sublattice [16].

Cite as: S. Rzayeva, Y. Yakubov, U. Khalilov, M. Aliyev, A.Sh. Asare, East Eur. J. Phys. 3, 251 (2026), https://doi.org/10.26565/2312-4334-2026-3-20

Motivated by these unresolved issues, the present work provides a systematic spin-polarized first-principles investigation of Au-doped SiC nanosheets. Single (1Au@Si) and double (2Au@2Si) substitutional doping configurations are examined using a large 80-atom supercell to effectively suppress artificial dopant–dopant interactions and ensure reliable evaluation of intrinsic electronic and magnetic properties. The calculations were performed within the framework of spin-polarized density functional theory using the QuantumATK simulation platform [17], employing the LDA+U formalism to account for localized electronic states and reduce self-interaction effects [19–21].

Our calculations reveal a dual and nontrivial impact of Au incorporation on the electronic and magnetic behavior of SiC nanosheets. First, Au substitution induces a pronounced band-gap narrowing while largely preserving spin-degenerate band dispersions, thereby maintaining the semiconducting nature of the host material. Second, Au doping stabilizes a localized ferrimagnetic-like spin state that is not manifested through conventional exchange splitting in the band structure, but is instead primarily revealed by atom-resolved Mulliken spin population analysis.

Notably, the induced magnetism is found to be predominantly mediated by the carbon sublattice, which hosts sizable positive local magnetic moments. In contrast, the Au dopants and their nearest-neighbor Si atoms contribute antiparallel, compensating spin polarization. For the 1Au@Si configuration, a net magnetic moment of approximately $3\mu_B$ is obtained, whereas double Au substitution stabilizes a robust magnetic state with a total magnetic moment of about $6\mu_B$. Importantly, the 2Au@2Si system converges to essentially the same magnetic solution irrespective of whether the calculations are initialized in non-magnetic, ferromagnetic (FM), or antiferromagnetic (AFM) spin configurations. This behavior indicates that the magnetic ground state is intrinsically governed by dopant–host hybridization effects rather than by externally imposed spin ordering, a characteristic feature commonly observed in transition-metal- and noble-metal-modified semiconductors and dilute magnetic systems [6,15,16,25].

Taken together, these results establish Au-doped SiC nanosheets as a promising class of two-dimensional dilute magnetic semiconductors in which band-gap engineering and thermally robust magnetism can coexist. Such coexistence of semiconducting character and localized magnetic ordering is particularly desirable for next-generation spintronic and multifunctional nanoelectronic applications, where spin-dependent electronic transport and stable magnetic ordering are essential [2,3,9,11].

In addition to inducing robust spin polarization, Au substitution is found to stabilize a high-temperature magnetic phase in SiC nanosheets. Total-energy comparisons between non-magnetic, ferromagnetic, and antiferromagnetic configurations reveal that spin-polarized states are energetically favored, with a very small energy splitting between FM and AFM solutions, indicating near magnetic degeneracy. Mean-field estimation based on first-principles total-energy differences yields an estimated Curie temperature of approximately 510 K. Within the limitations of the mean-field approximation, this result suggests the possibility of magnetic stability above room temperature. This result demonstrates that Au-doped SiC nanosheets can simultaneously exhibit semiconducting character and thermally robust magnetism, a combination rarely achieved in two-dimensional dilute magnetic semiconductors and highly desirable for practical spintronic device applications [2,6,9,11,23].

2. COMPUTATIONAL METHODOLOGY

All calculations were carried out within the framework of spin-polarized density functional theory (DFT) using the linear combination of atomic orbitals (LCAO) method, as implemented in the Quantum ATK simulation package [17-18]. Spin polarization was explicitly accounted for to accurately describe dopant-induced magnetic effects and spin-dependent electronic reconstruction in SiC nanosheets.

Within the spin-polarized DFT+U formalism, the total electronic charge density was decomposed into spin-up (α) and spin-down (β) components. The spin density, defined as the difference between these two spin channels, was used to characterize the system's magnetic response and spin polarization. The corresponding relations are given by:

$$\rho(r) = \rho^{\alpha}(r) + \rho^{\beta}(r) \quad (1)$$

$$\Delta\rho(r) = \rho^{\alpha}(r) - \rho^{\beta}(r) \quad (2)$$

Here, $\rho^{\alpha}(r)$ and $\rho^{\beta}(r)$ denote the spin-up and spin-down electron densities, respectively, while $\Delta\rho(r)$ represents the spin density distribution, which provides direct insight into the origin and spatial distribution of magnetism in the doped SiC nanosheets.

Exchange-correlation effects were described within the local density approximation (LDA) using the Perdew-Zunger parameterization of the Ceperley-Alder data [20]. To reduce the self-interaction error inherent in conventional LDA calculations, the rotationally invariant Dudarev DFT+U formalism was employed. Consistent with previous theoretical studies, the effective on-site Coulomb parameters were chosen as USi = 5.0 eV for Si-3d states and UC = 4.8 eV for C-2p states. These values provide a physically reasonable description of the electronic and magnetic properties of Au-doped SiC nanosheets.

Core-valence interactions were treated by norm-conserving pseudopotentials of the Fritz Haber Institute (FHI) type [18]. The valence electronic states of all constituent elements (Si, C, and Au) were expanded using a double-zeta polarized (DZP) numerical atomic orbital basis set, providing a reliable and balanced description of both the light host atoms and the heavy Au dopants [20].

Electronic occupations were determined using the Fermi–Dirac distribution with an electronic temperature of 300 K to ensure numerical stability and smooth convergence of the self-consistent field cycles. A real-space density mesh cutoff of 75 Hartree was employed, which was found to be sufficient to achieve well-converged total energies and charge density distributions for all studied configurations.

Brillouin-zone integrations were performed using a Monkhorst-Pack k-point mesh of 3x3x1, which provides a suitable compromise between numerical accuracy and computational efficiency for the employed supercell size [22]. The two-dimensional SiC nanosheet was modeled using a 4×4 hexagonal supercell containing 80 atoms (40 Si and 40 C). A vacuum region of at least 15 Å was introduced perpendicular to the nanosheet plane to suppress spurious interactions between periodically repeated images.

Substitutional Au doping was realized by replacing Si atoms, considering both the single-dopant 1Au@1Si configuration (≈1.25 at.%) and the double-dopant 2Au@2Si configuration (≈2.50 at.%). The dopant concentration was defined relative to the total number of atoms in the supercell [21]. For the 2Au@2Si system, spin-unconstrained as well as ferromagnetic (FM) and antiferromagnetic (AFM) initial spin configurations were explicitly examined to evaluate the stability and robustness of the magnetic ground state. All atomic structures were fully optimized using a conjugate-gradient algorithm until the residual forces on each atom were reduced below 0.01eV $Å^{-1}$ and the total energy convergence criterion reached 10-5eV. Spin-resolved band structures were calculated along the Γ–Z direction, with the Fermi level set to 0eV. In addition, the total and partial densities of states (TDOS and PDOS) were evaluated to analyze dopant-induced impurity states and Au–host hybridization effects [19,20].

To elucidate the microscopic origin of magnetism in Au-doped SiC nanosheets, Mulliken spin population analysis was employed. Within this framework, the local magnetic moment associated with a given atom A is defined as the difference between its spin-up and spin-down Mulliken populations:

$$\mu_A = n_A^{\alpha} - n_A^{\beta} \tag{3}$$

where n_A^{α} and n_A^{β} represent the Mulliken populations of spin-up and spin-down electrons localized on atom A, respectively. The total magnetic moment of the supercell is then obtained by summing the atomic contributions over all atoms:

$$\mu_{tot} = \sum_A \mu_A \tag{4}$$

This analysis is particularly important for the present system, as Au-doped SiC nanosheets exhibit spin-degenerate band structures while simultaneously sustaining a finite net magnetic moment. Such behavior cannot be fully resolved from band structure analysis alone. Mulliken spin population analysis enables direct identification of the dominant spin carriers and provides atom-resolved insight into the system's magnetic texture. The results suggest that the induced magnetism is predominantly localized on the carbon sublattice, whereas the Au dopants and neighboring Si atoms contribute smaller, anti-parallel spin moments that partially compensate the total magnetization. This finding highlights the crucial role of dopant–host hybridization in mediating magnetism through the surrounding lattice rather than through localized Au moments alone.

For systems with identical chemical composition, such as the 2Au@2Si configuration, the relative stability of different magnetic solutions was evaluated by comparing their total energies. The magnetic stabilization energy was defined as:

$$\Delta E_{mag} = E_{NM} - E_{FM}, \tag{5}$$

where E_{NM} and E_{FM} denote the total energies of the non-magnetic and ferromagnetic states, respectively. A positive value of ΔE_{mag} indicates that the ferromagnetic solution is energetically favored over the non-magnetic one.
In addition, the energy difference between antiferromagnetic and ferromagnetic configurations,

$$\Delta E_{AFM-FM} = E_{AFM} - E_{FM}, \tag{6}$$

was calculated to assess the sensitivity of the magnetic ground state to the initial spin ordering. The small energy separation observed between the FM and AFM solutions indicates a near-degeneracy of these magnetic states. Such behavior suggests that the Au-induced magnetism is not governed by rigid long-range ferromagnetic coupling but instead reflects a ferrimagnetic-like or weakly competing magnetic ordering mediated by the Si-C host lattice. This energetic proximity suggests that the dopant-induced magnetic state is largely governed by dopant–host hybridization in Au-substituted SiC nanosheets.

3. RESULTS AND DISCUSSION

3.1. Electronic structure of Au-doped SiC nanosheets

The electronic band structures of Au-doped SiC nanosheets were systematically analyzed to elucidate the influence of Au concentration on the system's electronic properties [22,23]. Two substitutional doping configurations were considered: a single Au atom substituting a Si site (SiC:1Au@1Si NS) and a double Au substitution at two Si sites (SiC:2Au@2Si NS), which serve as representative models for low and moderate dopant concentrations in two-dimensional SiC systems [24].

Spin-polarized band structures were calculated along the high-symmetry path Γ–Z of the 2D Brillouin zone, with the Fermi level aligned at 0eV, following standard electronic-structure analysis protocols for a two-dimensional Brillouin zone (2D monolayer). The corresponding results are presented in Figures 1 and 2.

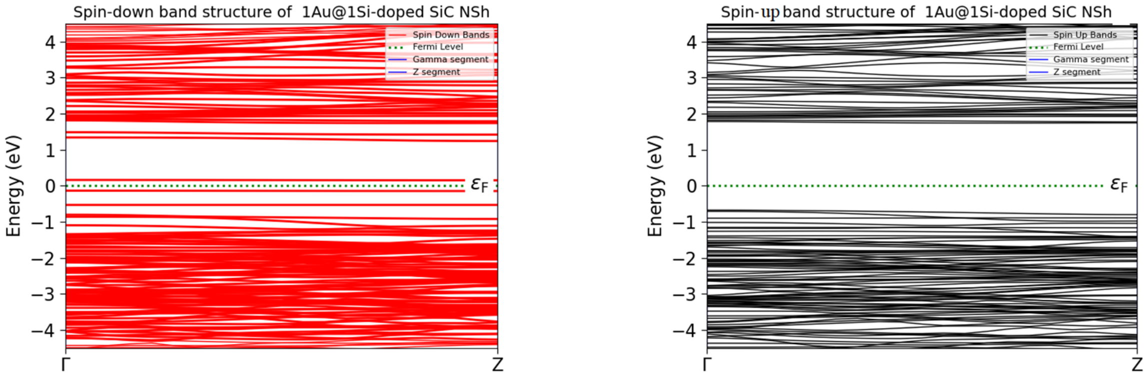

Figure 1. Spin-polarized electronic band structures of the 1Au@1Si-SiC nanosheet along the Γ-Z direction

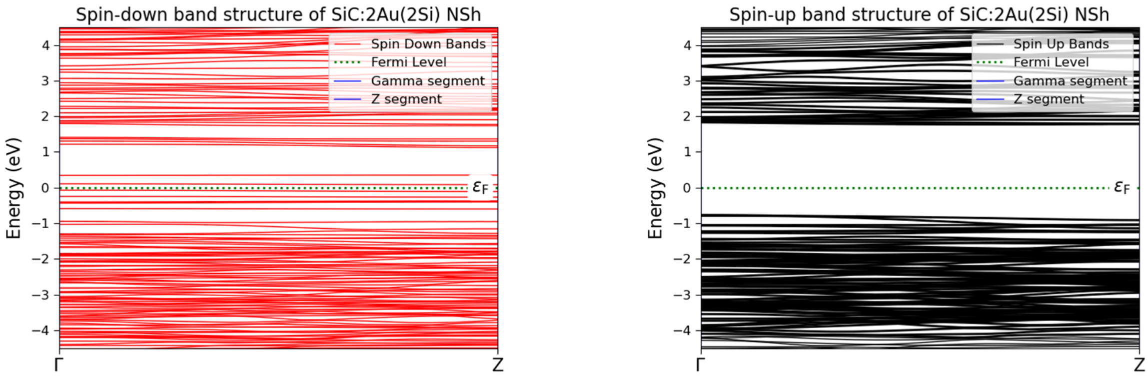

Figure 2. Spin-polarized electronic band structures of the SiC:2Au(2Si) nanosheet along the Γ-Z direction

As shown in Figure 1, the SiC:1Au@1Si nanosheet retains a semiconducting character in both spin-up and spin-down channels, exhibiting a narrow band gap of approximately 0.30 eV. This behavior is consistent with previous reports on noble-metal-induced band-gap modulation in wide-band-gap semiconductor systems. Upon increasing the Au concentration to the SiC:2Au@2Si configuration, a pronounced reduction of the band gap is observed, yielding values of approximately 0.18eV (direct) and 0.16eV (indirect), as summarized in Table 1.

Table 1. Spin-resolved band gaps and band-edge positions (VBM and CBM) for SiC:1Au@1Si and SiC:2Au@2Si nanosheets, illustrating Au-concentration-induced band gap narrowing while preserving spin degeneracy.

System	Spin channel	Direct band gap (eV)	Indirect band gap (eV)	VBM (eV)	CBM (eV)
SiC:1Au(1Si) NS	Spin-up	0.297	0.288	-0.1389	0.1491
	Spin-down	0.297	0.288	-0.1389	0.1491
SiC:2Au(2Si) NS	Spin-up	0.179	0.157	-0.0738	0.0824
	Spin-down	0.179	0.157	-0.0738	0.0824

The observed dopant-concentration-dependent band gap narrowing originates from an upward shift of the valence band maximum (VBM), accompanied by a downward shift of the conduction band minimum (CBM). This effect can be attributed to enhanced hybridization between Au-derived states and the host Si–C orbitals, which modifies the electronic structure near the Fermi level [25].

Importantly, the spin-up and spin-down band dispersions remain largely similar for both doping configurations, indicating the absence of pronounced exchange splitting at the band-dispersion level. This behavior reflects the closed-shell electronic configuration of Au and suggests that Au substitution primarily modifies the electronic structure through orbital hybridization rather than inducing strong band-resolved spin asymmetry. Nevertheless, as discussed in Section 3.2, atom-resolved spin population analysis reveals the emergence of dopant-induced magnetic moments mediated by the host lattice. Such behavior is consistent with previous first-principles studies on noble-metal-doped wide-band-gap semiconductor systems [23,24,26].

To further elucidate the effect of Au incorporation on the electronic structure, the total density of states (TDOS) was systematically analyzed for both single and double Au-doped SiC nanosheets. As shown in Figure 3, pristine SiC nanosheets exhibit a clear semiconducting gap around the Fermi level (E_F=0eV), which is in good agreement with previous first-principles studies on two-dimensional SiC monolayers [30].

Upon single Au substitution, impurity-induced states emerge near the valence- and conduction-band edges, leading to a pronounced enhancement of the TDOS in the vicinity of the Fermi level while preserving a finite band gap. These states mainly originate from hybridization between Au-derived orbitals and neighboring Si and C states, resulting in band-gap narrowing without altering the overall semiconducting character of the system. When the Au concentration is increased to the double-doped configuration (Figure 4), a further increase in the TDOS near EF is observed, accompanied by broader spectral features. This behavior reflects stronger Au-Au and Au-host interactions as well as enhanced electronic delocalization at higher dopant concentrations.

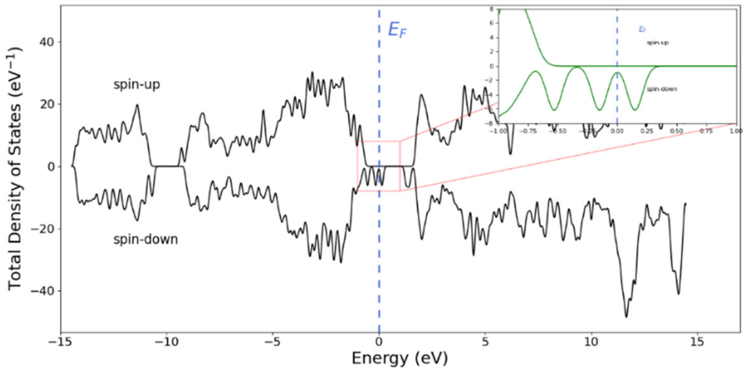

Figure 3. TDOS of single Au-doped SiC ($Au_1Si_{39}C_{40}$). The dashed line indicates the Fermi level (EF = 0eV).

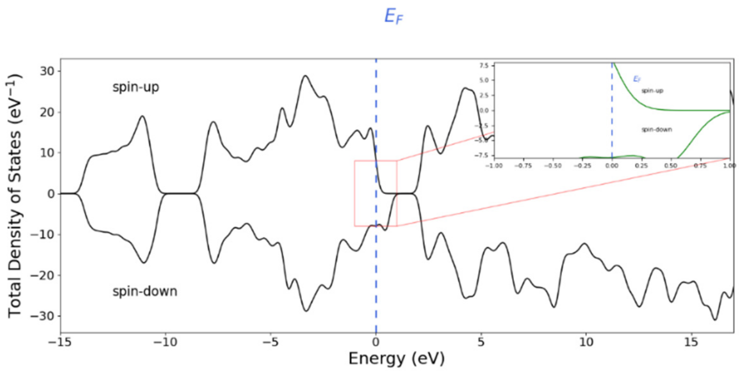

Figure 4. TDOS of double Au-doped SiC ($Au_2Si_{38}C_{40}$), showing enhanced states near E_F compared to the single-doped case

Despite the increased density of states near the Fermi level, both Au-doped systems remain semiconducting, with no finite TDOS appearing exactly at E_F.

Moreover, the spin-up and spin-down TDOS curves remain largely symmetric, indicating no pronounced spin asymmetry at the TDOS level, indicating that Au incorporation modifies the electronic structure without inducing a semiconductor-to-metal transition.

Although the spin-up and spin-down TDOS curves remain largely similar over the entire energy range, enlarged DOS plots near the Fermi level reveal weak spin-dependent differences. These small asymmetries indicate that the exchange splitting is relatively weak and localized. Therefore, the finite magnetic moments obtained from Mulliken population analysis originate primarily from localized spin polarization rather than from pronounced exchange splitting throughout the entire electronic structure.

This nearly spin-degenerate electronic structure is consistent with previous first-principles investigations of noble-metal-doped semiconductors.

To identify the atomic and orbital origins of the electronic reconstruction induced by Au doping, spin-resolved partial density of states (PDOS) calculations was performed. Figure 5 shows the orbital-projected PDOS of Au in the single-Au-doped SiC nanosheet. The electronic states in the vicinity of the Fermi level are predominantly governed by Au-5d orbitals, while the contributions from Au-6s and Au-6p states are comparatively weaker and distributed over a broader energy range. The spin-up and spin-down PDOS curves remain largely similar over most of the energy range, indicating weak exchange splitting, consistent with the closed-shell electronic configuration of Au and previous first-principles studies [28,29]. However, enlarged views near the Fermi level reveal small spin-dependent differences, indicating weak local spin polarization. The Au-5d states dominate the electronic states near E_F and contribute to the localized magnetic behavior.

For the double-Au-doped configuration (Figure 6), the Au-5d states become more intense and exhibit notable broadening, reflecting enhanced dopant-dopant as well as dopant-host interactions at higher Au concentration. Despite this increased electronic hybridization, spin degeneracy remains preserved, further reinforcing the conclusion that Au acts primarily as a modifier of the electronic structure rather than as a magnetic impurity in SiC nanosheets.

Although the overall exchange splitting remains relatively weak, the observed spin-dependent differences support the existence of localized magnetic polarization, consistent with the Mulliken spin population analysis.

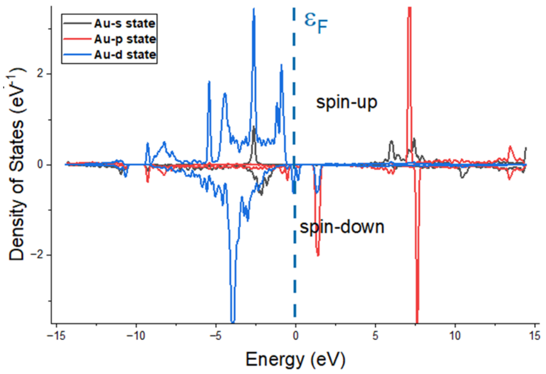

Figure 5. Spin-resolved PDOS of Au orbitals in single Au-doped SiC (Au1Si39C40)

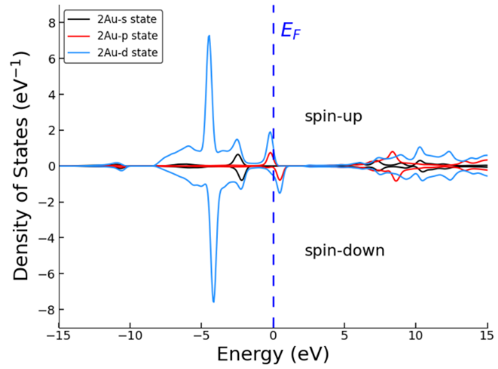

Figure 6. Spin-resolved PDOS of Au orbitals in double Au-doped SiC ($Au_2Si_{38}C_{40}$)

The spin-resolved partial density of states (PDOS) of host carbon atoms is presented in Figure 7. The electronic states near the valence and conduction band edges are predominantly governed by C-2p orbitals, whereas the C-2s and C-2d states contribute mainly at lower binding energies.

Although the total C-PDOS remains nearly symmetric, several carbon atoms neighboring the Au dopants exhibit substantial local magnetic moments according to the Mulliken analysis. This indicates that the induced magnetism is highly localized and cannot be fully resolved from orbital-averaged PDOS alone.

A similar trend is observed for the host silicon atoms, as shown in Figure 8. The Si–3p orbitals provide the dominant contributions to both the valence and conduction bands, while the Si–3d states exhibit only weak and broadly distributed features across the energy spectrum. The nearly symmetric spin-resolved PDOS indicates that Si atoms do not exhibit pronounced spin polarization, despite the pronounced Au-induced electronic reconstruction. These results highlight that the role of the host atoms is primarily indirect, mediated through orbital hybridization with Au states rather than through the development of substantial local magnetic moments.

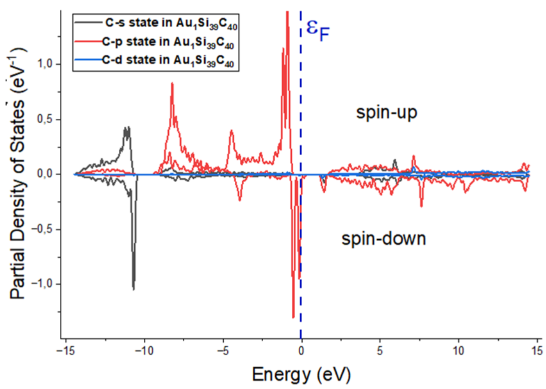

Figure 7. Spin-resolved partial density of states (PDOS) of C-s, C-p, and C-d orbitals for the $Au_1Si_{39}C_{40}$ system

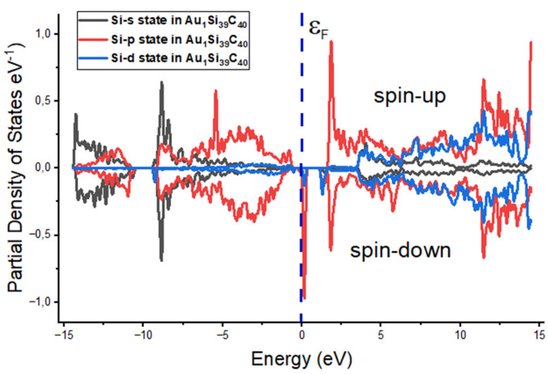

Figure 8. Spin-resolved partial density of states (PDOS) of Si-s, Si-p, and Si-d orbitals for the $Au_1Si_{39}C_{40}$ system

To quantitatively assess the influence of Au concentration on the electronic band gap characteristics of SiC nanosheets, the spin-resolved band gaps were systematically evaluated for pristine, single-Au-doped, and double-Au-doped configurations. Particular attention was paid to the evolution of both direct and indirect band gaps in the spin-up (↑) and spin-down (↓) channels in order to clarify whether Au incorporation induces spin asymmetry or magnetic exchange effects. Increasing Au concentration results in pronounced narrowing of both direct and indirect band gaps while preserving identical spin-up and spin-down values, demonstrating that Au enables effective band gap engineering in SiC nanosheets while preserving nearly spin-degenerate electronic states and only weak exchange splitting.

3.2. Magnetic Properties of Au-Doped SiC Nanosheets

3.2.1. Pristine 80-Atom SiC Nanosheet: Non-Magnetic Reference State

The magnetic properties of the pristine 80-atom SiC nanosheet were first investigated using spin-polarized Mulliken population analysis to establish a reliable non-magnetic reference state. As shown in Fig. 9, the pristine system exhibits negligible spin polarization at all atomic sites, with local magnetic moments confined within $\pm 0.01\mu_B$. Silicon atoms carry very small positive magnetic moments ($\approx +0.011$-$0.012\mu_B$), whereas carbon atoms display comparably small negative moments (≈ -0.010 to $-0.013\mu_B$), resulting in an almost perfect compensation between the two sublattices.

Consequently, the total Mulliken spin magnetic moment converges to approximately zero ($\Sigma_\mu \approx -0.000\mu_B$), as summarized in Table 2, confirming the absence of intrinsic magnetism in the pristine nanosheet. These extremely small residual moments fall well within the numerical uncertainty associated with Mulliken charge and spin partitioning and therefore cannot be interpreted as evidence of genuine magnetic ordering.

Further orbital-resolved analysis reveals spin-symmetric occupations of the Si s/p and C p states, with no observable exchange splitting near the Fermi level. Overall, these findings demonstrate that pristine SiC nanosheets possess a fully spin-degenerate, non-magnetic ground state, in excellent agreement with previous first-principles studies on two-dimensional SiC systems [30,31]. This non-magnetic reference state provides a robust baseline for identifying and quantitatively assessing dopant-induced magnetism upon Au substitution.

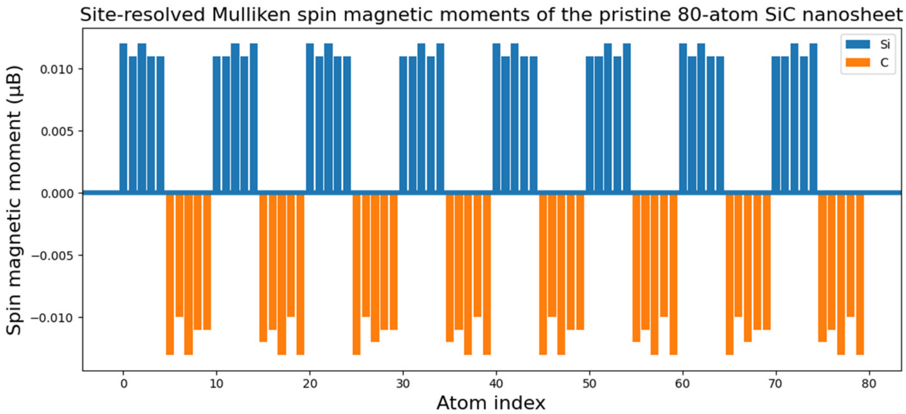

Figure 9. Site-resolved Mulliken spin magnetic moments of the pristine 80-atom SiC nanosheet, showing complete compensation between Si and C contributions and a vanishing net magnetic moment

Table 2. Element-resolved Mulliken spin magnetic moments for the pristine 80-atom SiC nanosheet

Element	Number of atoms	Spin moment range (μ_B)	Total contribution (μ_B)
Si	40	+0.011 to +0.012	≈ +0.48
C	40	-0.010 to -0.013	≈ -0.48
Total	80	—	0.000

3.2.2. Single Au Substitution: 1Au@1Si Configuration

The substitution of a single Si atom by Au induces a pronounced magnetic response in the SiC nanosheet. The atom-resolved Mulliken spin magnetic moments shown in Fig. 10 reveal a strongly inhomogeneous and localized spin distribution, which is characteristic of induced magnetism governed by dopant–host interactions. The total magnetic moment reaches approximately 3.00 μB, indicating the emergence of a ferromagnetic-like state (Tables 3 and 4).

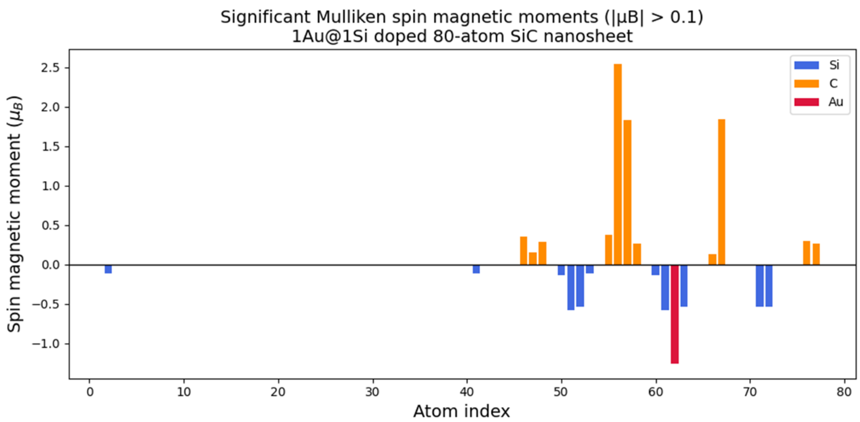

Figure 10. Atom-resolved Mulliken spin magnetic moments for the 1Au@1Si-doped SiC nanosheet

Table 3. Element-resolved Mulliken spin magnetic moments for the 1Au@1Si configuration

Element	Number of atoms	Sum of spin moments (μ_B)	Mean per atom (μ_B)	Max |moment| (μ_B)	Min (μ_B)	Max (μ_B)
C	40	8.781	0.2195	2.543	-0.011	2.543
Si	39	-4.520	-0.1159	0.583	-0.583	0.001
Au	1	-1.254	-1.2540	1.254	-1.254	-1.254
Total	80	≈ 3.00				

The reported total spin moment is 3.003μ_B. Minor deviations on the order of $10^{-3}\mu_B$ arise from rounding of atom-resolved values.

Table 4. Dominant spin-carrying atoms in the 1Au@1Si configuration

Atom index	Element	Spin moment (μ_B)
56	C	+2.543
67	C	+1.839
57	C	+1.834
62	Au	-1.254
51	Si	-0.583
61	Si	-0.581
52	Si	-0.541
63	Si	-0.537
71	Si	-0.531
72	Si	-0.531
55	C	+0.379
46	C	+0.348

Notably, the Au dopant itself carries a sizable negative local magnetic moment (−1.25 μB), whereas several neighboring carbon atoms exhibit unusually large positive moments exceeding +2.5 μB. The unusually large Mulliken moments obtained for several carbon atoms should be interpreted with caution because Mulliken populations depend on the employed basis set and population scheme.

This behavior suggests that the dominant magnetic contribution does not originate from the Au atom but is instead mediated by the surrounding carbon sublattice through strong Au–C hybridization. Such a redistribution of spin density is commonly associated with induced magnetism in doped sp-electron systems [32,33].

In contrast, silicon atoms acquire relatively small antiparallel magnetic moments, acting as a compensating magnetic background. Element-resolved analyses (Figs. 11 and 12) confirm that carbon provides the dominant positive contribution to the net magnetization, while both Si and Au contribute negatively. Atoms located far from the dopant site exhibit near-zero spin magnetic moments, confirming the localized nature of the magnetic perturbation.

These results demonstrate that even a single Au substitution is sufficient to generate robust magnetism in SiC nanosheets. Importantly, the magnetization is largely delocalized over the carbon framework rather than being confined to the heavy dopant atom, highlighting the central role of host-mediated spin polarization in Au-doped SiC systems [34,35].

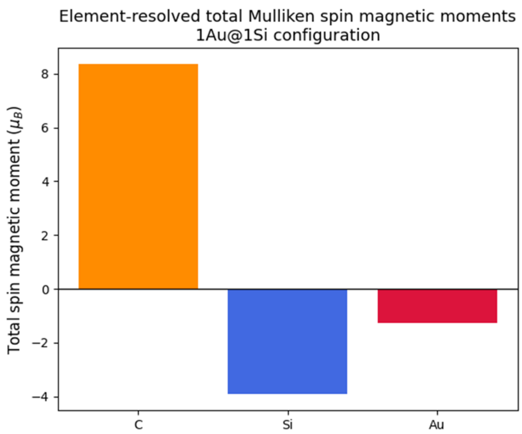

Figure 11. Element-resolved total Mulliken spin magnetic moments for the 1Au@1Si configuration

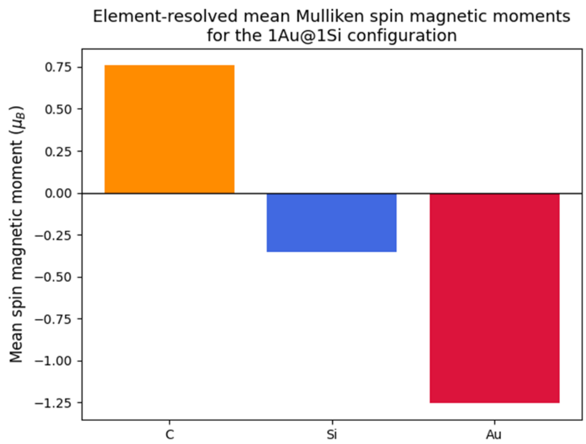

Figure 12. Element-resolved mean Mulliken spin magnetic moments for the 1Au@1Si-doped SiC nanosheet

3.2.3. Double Au Substitution: 2Au@2Si Configuration (General State)

Spin-polarized calculations for the 2Au@2Si configuration reveal a further enhancement of the magnetic response compared to the single-dopant case. As shown in Fig. 13, only a limited number of atoms exhibit significant local magnetic moments ($|\mu| > 0.1\mu_B$), indicating a highly localized yet intensified induced magnetism mechanism. The largest positive magnetic moments are predominantly localized on carbon atoms, reaching values of up to +2.41μ_B, whereas silicon atoms and Au dopants exhibit negative (antiparallel) spin polarization.

Element-resolved integration (Fig. 14 and Table 5) demonstrates that carbon provides a large positive total spin magnetic moment (+19.06μ_B), while silicon (−10.44μB) and gold (−2.62μ_B) contribute compensating negative moments. The incomplete cancellation between these opposing sublattices results in a finite net magnetic moment of approximately 6.01μ_B, confirming the stabilization of a ferrimagnetic-like ground state.

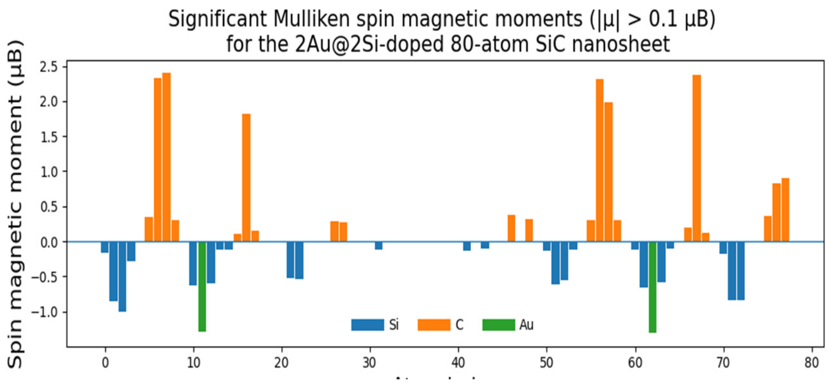

Figure 13. Local Mulliken spin magnetic moments for the 2Au@2Si-doped SiC nanosheet ($|\mu| > 0.1\mu_B$)

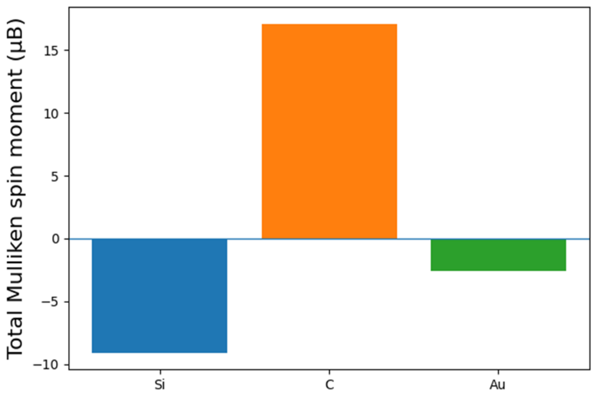

Figure 14. Element-resolved total Mulliken spin magnetic moments for the 2Au@2Si configura-tion

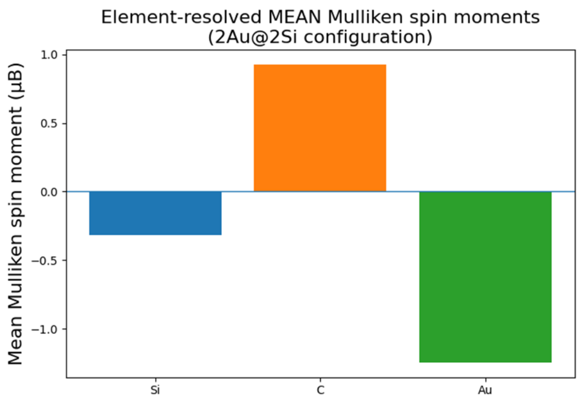

Figure 15. Element-resolved mean Mulliken spin magnetic moments for the 2Au@2Si-doped SiC nanosheet

Table 5. Element-resolved magnetic characteristics of the 2Au@2Si-doped 80-atom SiC nanosheet

Element	Number of atoms	Total spin moment (μ_B)	Mean spin moment per atom (μ_B/atom)	Maximum (μ_B)	Dominant spin role
C	40	+19.059	+0.476	+2.410	Primary spin polarization carrier
Si	38	-10.437	-0.275	-1.005	Antiparallel (compensating) host
Au	2	-2.616	-1.308	-1.319	Dopant-induced antiparallel center
Total (Sum)	80	+6.007	-	-	Net ferromagnetic moment

3.2.4. Ferromagnetic and AFM-Initialized 2Au@2Si Configuration: Robust Carbon-Mediated Induced Ferrimagnetism and Spin-Compensation Mechanism

When the 2Au@2Si-doped 80-atom SiC nanosheet is initialized in a ferromagnetic (FM) state, the system converges to a stable spin-polarized solution with a net magnetic moment of $\Sigma\mu \approx 6.007$ μB. This behavior demonstrates that Au substitution induces an intrinsic magnetic response rather than a metastable artifact associated with the initial spin configuration (Tables 6 and 7). Atom-resolved Mulliken spin magnetic moments reveal that the magnetization is highly nonuniform and predominantly localized on a limited number of lattice sites in the vicinity of the do-pant-induced perturbation. The largest positive moments are hosted by carbon atoms (e.g., C7 ≈ +2.404 μ_B, $C_{67} \approx +2.372\mu_B$, $C_6 \approx +2.331\mu_B$, $C_{56} \approx +2.317\mu_B$, $C_{57} \approx +1.983\mu_B$, and $C_{16} \approx +1.821\mu_B$), as summarized in Table 10 and illustrated in Figures 16-18.

This pronounced localization on the carbon sublattice is physically consistent with a carbon-mediated induced-magnetism mechanism. Au substitution at Si sites perturbs the local bonding environment and electronic potential landscape, leading to reconstruction and spin splitting of C-p–dominated electronic states near the Fermi level. Within this mechanism, the dopant primarily acts as a spin polarizer that enables exchange-driven imbalance in the host electronic states, while the carbon sublattice becomes the principal reservoir of positive spin density. Element-resolved total moments corroborate this interpretation, showing that carbon provides the dominant positive contribution ($\Sigma\mu(C) \approx +19.057\mu_B$), whereas the silicon framework and Au dopants contribute antiparallel (negative) polarization ($\Sigma\mu(Si) \approx -10.450$ μ_B and $\Sigma\mu(Au) \approx -2.599\mu_B$), as reported in Table 7.

Table 6. Statistical summary of selected atom-resolved Mulliken local spin magnetic moments (μ_B) for the FM-initialized 2Au@2Si-doped SiC nanosheet

Descriptor	Local moment (μ_B)	Atom(s)/index(es)	Brief comment
Au (mean)	-1.300	Au(11)=-1.287, Au(62)=-1.312	Au dopants align antiparallel to the net magnetization
Au_1	-1.287	Au(11)	Substitutional Au at Si site
Au_2	-1.312	Au(62)	Substitutional Au at Si site
C (maximum)	+2.404	C(7)	Strong Au-C hybridization, dominant spin polarization
C (high values)	+2.372, +2.331, +2.317, +1.983, +1.821	C(67), C(6), C(56), C(57), C(16)	Majority of magnetization localized on the C sublattice
Si (largest |μ|)	-0.998	Si(2)	Si sublattice provides compensating (antiparallel) contribution
Si (smallest |μ|)	-0.005	Si(34)	Near-zero moment, weak spin polarization
Total moment (sum)	6.007	-	Net magnetization: FM, ferrimagnetic-like distribution

Table 7. Element-resolved Mulliken spin magnetic moments for the FM 2Au@2Si–SiC nanosheet.

Element	Number of atoms	Total spin moment (μ_B)
C	40	19.0570
Si	38	-10.4500
Au	2	-2.5990

This antiparallel partitioning is also reflected in the element-resolved mean magnetic moments (Figures 16 and 17), indicating that Si and Au atoms do not suppress the magnetization but instead participate through spin compensation. Specifically, they develop induced negative moments that partially offset the strong carbon-derived magnetization. Such a compensated spin arrangement is most appropriately described as ferromagnetic-like, since different sublattices carry oppositely oriented spin polarization whose magnitudes do not fully cancel, resulting in a finite net magnetic moment.

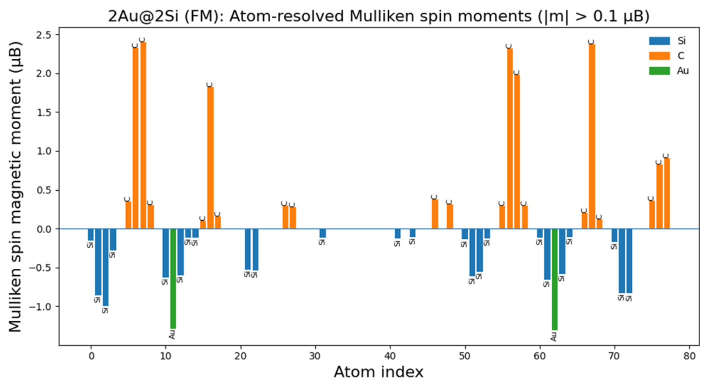

Figure 16. Element-resolved mean spin magnetic moments. Carbon atoms exhibit a dominant positive contribution that governs the ferromagnetic net response, while Si and Au show antiparallel (negative) polarization, providing partial compensation

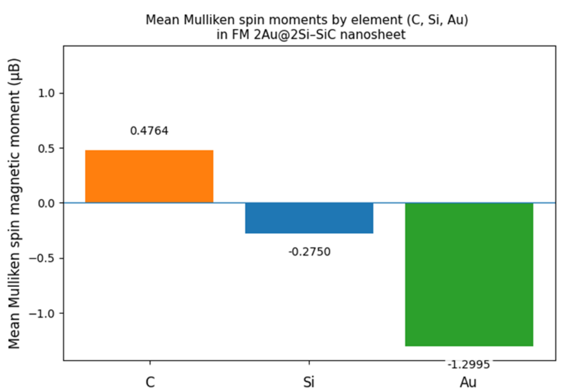

Figure 17. Element-resolved mean Mulliken spin magnetic moments for the FM 2Au@2Si-doped SiC nanosheet, showing positive spin polarization on C atoms and compensating negative moments on Si and Au, with Au contributing the largest negative component

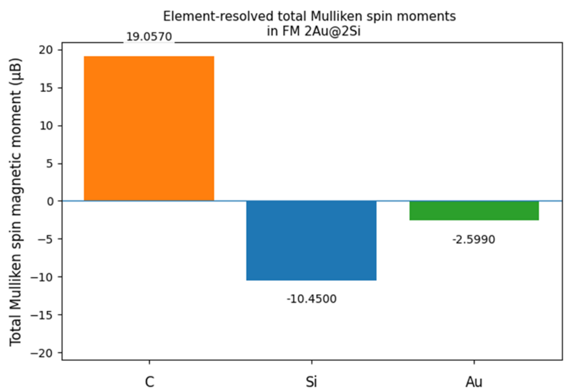

Figure 18. Element-resolved Mulliken spin magnetic moments for the FM 2Au@2Si configuration, showing a dominant positive contribution from the carbon sublattice and compensating anti-parallel moments on Si and Au atoms

A critical stability test is provided by the antiferromagnetic (AFM) initialization. If the magnetism were merely an imposed FM solution, an AFM initial condition would be expected to relax toward a compensated AFM state ($\Sigma\mu \rightarrow 0$) or to a qualitatively different local-moment distribution. Instead, the AFM-initialized calculation converges to essentially the same non-compensated magnetic solution with $\Sigma\mu \approx 6.007\mu_B$ (Table 8), demonstrating that the magnetic ground state is robust against the initial magnetic ordering and is dictated by intrinsic dopant–host interactions.

Table 8. Element-wise summary of Mulliken magnetic moments for the AFM 2Au@2Si–SiC nanosheet

Element	Number of atoms (N)	Total magnetic moment, Σμ (μB)	Mean magnetic moment, ⟨μ⟩ (μB/atom)	Mean |μ| (μB/atom)	Minimum μ (μB)	Maximum μ (μB)
Au	2	−2.596	−1.298	1.298	−1.310	−1.286
C	40	+19.055	+0.476	0.477	−0.003	+2.397
Si	38	−10.452	−0.275	0.275	−0.997	−0.005
Total	80	+6.007	—	—	—	—

Atom-resolved AFM moments (Figure 19 and Table 9) confirm that the largest positive moments remain localized on carbon sites (maximum ≈+2.397μ_B on C7, followed by ≈ +2.374 μ_B on C_{67} and ≈+2.335μ_B on C_6), while both Au dopants retain sizeable antiparallel moments (Au_{11} ≈-1.286 μ_B and Au_{62} ≈ -1.310μ_B). Silicon atoms again act as distributed compensating centers, with the largest magnitude observed at Si2 (≈-0.997μ_B).

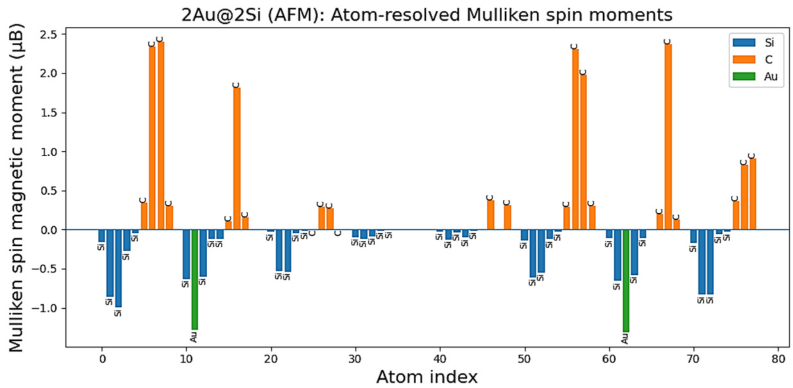

Figure 19. Atom-resolved Mulliken spin magnetic moments for the AFM-initialized 2Au@2Si–SiC nanosheet

Table 9. Statistical summary of selected atom-resolved Mulliken local spin magnetic moments (μB) for the AFM-initialized 2Au@2Si-doped SiC nanosheet

Descriptor	Local moment (μB)	Atom(s)/index(es)	Brief comment
Au (mean)	-1.298	Au(11) = -1.286, Au(62) = -1.310	Au dopants polarize in an antiparallel direction
Au_1	-1.286	Au(11)	Substitutional Au at a Si site
Au_2	-1.310	Au(62)	Substitutional Au at a Si site
C (maximum)	+2.397	C(7)	Strong Au–C hybridization, dominant spin polarization
C (high values)	+2.374, +2.335, +2.313, +1.980, +1.819	C(67), C(6), C(56), C(57), C(16)	Majority of the magnetization is localized on the carbon sublattice
Si (largest |μ|)	−0.997	Si(2)	Si sublattice provides compensating (antiparallel) contribution
Si (smallest |μ|)	−0.005	Si(34)	Near-zero moment, weak spin polarization
Total moment (sum)	6.007	—	Finite net magnetic moment (based on total sum)

Element-resolved decomposition in the AFM state (Figures 20-21 and Table 9) quantitatively reproduces the FM partitioning: Σμ(C) ≈+19.055 μ_B, Σμ(Si) ≈-10.452 μ_B, and Σμ(Au) ≈-2.596μ_B, yielding the same net magnetic moment through incomplete sublattice cancellation.

This unified physical picture is reinforced by the comparative summary across the General, FM, and AFM solutions (Figure 22 and Table 10). The consistency of (i) the mean local moment on Au atoms (≈ -1.30μB), (ii) the maximum local moments on carbon atoms (≈+2.40μ_B), (iii) the ex-trema of Si moments (largest |μ| ≈ -1.0μB and smallest ≈ -0.005μB), and (iv) the total magnetic moment Σμ ≈ 6.0μ_B demonstrates that the magnetization is not confined to the dopant sites but is redistributed over the SiC lattice with a dominant carbon character.

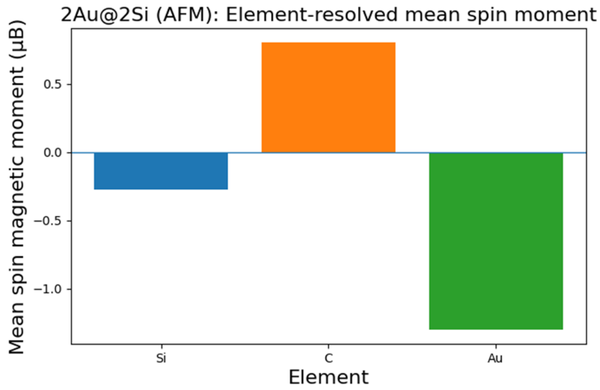

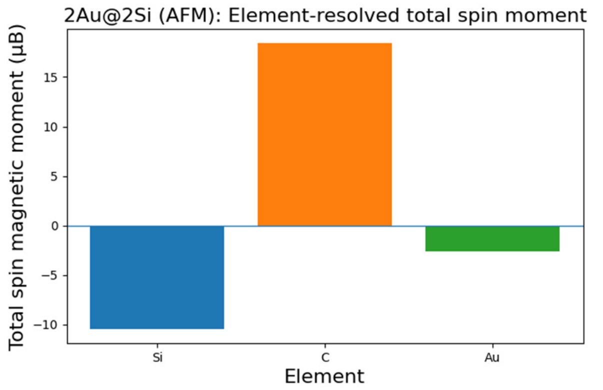

Figure 20. Element-resolved total Mulliken spin magnetic moments (μB): carbon provides a positive contribution, while silicon and gold contribute to compensating negative moments

Figure 21. Element-resolved mean Mulliken spin magnetic moments (AFM state)

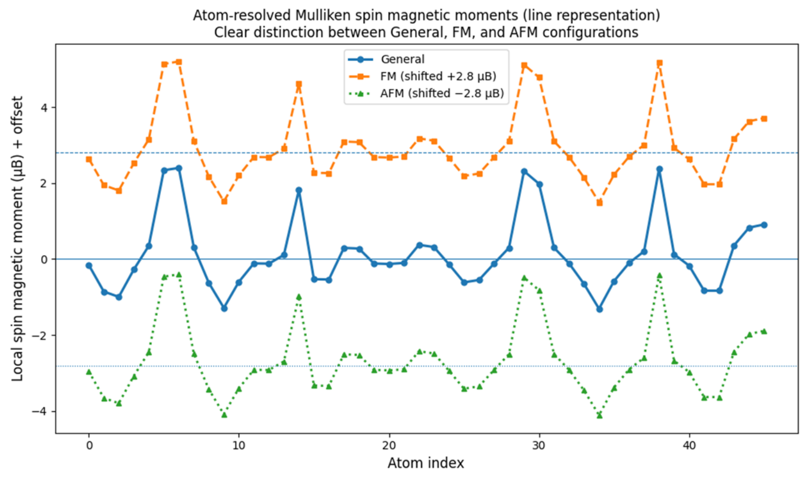

Figure 22. Atom-resolved Mulliken spin magnetic moments of the 2Au@2Si-doped SiC nanosheet comparing the general, FM, and AFM configurations

Table 10. Unified comparison of Mulliken spin magnetic moments for the 2Au@2Si–doped SiC nanosheet under General, FM, and AFM configurations

Quantity /Descriptor	General configuration	FM configuration	AFM configuration	Physical interpretation
Au (mean local moment, μ_B)	-1.298	-1.300	-1.298	Au dopants consistently show antiparallel polarization
Au1(μ_B)	-1.286 (Au_{11})	-1.287 (Au_{11})	-1.286 (Au_{11})	Substitutional Au at Si site
Au2(μ_B)	-1.310 (Au_{62})	-1.312 (Au_{62})	-1.310 (Au_{62})	Substitutional Au at Si site
C (maximum local moment, μ_B)	+2.410 (C7)	+2.404 (C_7)	+2.397 (C_7)	Strong Au-C hybridization, dominant spin polarization
C (other high local moments, μ_B)	+2.383, +2.331, +2.316, +1.998, +1.828	+2.372, +2.331, +2.317, +1.983, +1.821	+2.374, +2.335, +2.313, +1.980, +1.819	Spin density mainly localized on selected C atoms
Si (largest)	μ	(μ_B)	-1.005 (Si_2)	-0.998 (Si_2)
Si (smallest	μ	(μ_B)	-0.005 (Si_{34})	-0.005 (Si_{34})
Total moment Σμ (μ_B)	≈ 6.007	6.007	6.007	Robust net magnetic moment
Magnetic character	Ferrimagnetic-like	FM / ferrimagnetic-like	AFM-initialized → ferrimagnetic	Ground state is insensitive to initial spin ordering

From a spintronics perspective, this behavior is particularly advantageous. A robust, nonzero net magnetic moment that is insensitive to the initial spin configuration implies a stable magnetic response under perturbations, while the carbon-dominated spin polarization suggests that transport-relevant electronic states may acquire significant spin selectivity through host-state exchange splitting. Overall, the FM/AFM convergence behavior, together with the element-wise compensation pattern, provides strong evidence that Au substitution at Si sites stabilizes a carbon-driven, compensated ferrimagnetic-like magnetic ground state in SiC nanosheets, governed by induced spin polarization and dopant–host hybridization effects (Figures 16–21; Tables 5–9; Figure 22; Table 10) [30–44].

3.3. Curie Temperature Estimation and Magnetic Stability of Au-Doped SiC Nanosheets

In this section, the magnetic stability and Curie temperature–related characteristics of pristine and Au-substituted SiC nanosheets are systematically investigated within a first-principles framework. Spin-polarized density functional theory (DFT) calculations combined with Mulliken spin population analysis were employed to examine five representative configurations: pristine SiC nanosheet, single Au substitution at a Si site (1Au@1Si), double Au substitution at two Si sites (2Au@2Si) in the non-magnetic (NM) state, as well as ferromagnetic (FM) and antiferromagnetic (AFM) initializations of the same 2Au@2Si composition. This strategy enables a consistent assessment of dopant-induced magnetism and the energetic preference among different magnetic states under identical computational conditions.

The total energies of all configurations were calculated using the same computational parameters. For accurate total-energy comparisons, the electronic smearing was reduced to a very small value to minimize entropy-related contributions while maintaining numerical stability (Table 11). These energies form the basis for analyzing magnetic ordering and estimating the Curie temperature.

Table 11. Total energies of pristine and Au-substituted SiC nanosheets calculated under identical conditions for non-magnetic (NM), ferromagnetic (FM), and antiferromagnetic (AFM) states of the 2Au@2Si configuration

Configuration	Total energy (eV)
Pristine SiC nanosheet	-13295.45214
1Au1Si	-14484.79843
2Au(2Si)	-15514.21941
FM_2Au(2Si)	-15514.28516
AFM_2Au(2Si)	-15514.28677

It should be noted that direct comparison of absolute total energies between pristine, 1Au@1Si, and 2Au@2Si systems is not physically meaningful due to their different atomic compositions; such comparisons require a formation-energy analysis. In contrast, for the same 2Au@2Si composition, direct comparison among NM, FM, and AFM solutions is valid and allows reliable evaluation of magnetic stability [45].

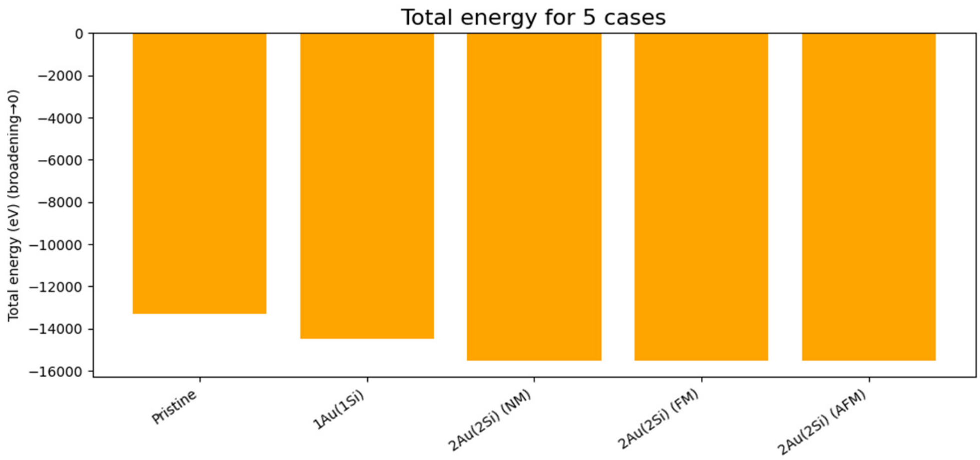

Figure 23. Total energy comparison for pristine SiC, 1Au@Si, and 2Au@2Si configurations in non-magnetic (NM), ferromagnetic (FM), and antiferromagnetic (AFM) states, showing energetic preference of magnetic solutions over the NM state for 2Au@2Si.

As summarized in Table 11 and illustrated in Figure 23, both magnetic solutions are significantly more stable than the non-magnetic reference state. The AFM initialization yields the lowest total energy, followed very closely by the FM state, establishing the energetic hierarchy

$$E_{AFM} < E_{FM} \ll E_{NM}$$

This result indicates that spin polarization provides a substantial stabilization of the Au-doped system, while the precise spin alignment plays a secondary role.

The energy gain associated with the onset of magnetism, which quantifies the stabilization of the magnetic phase, is defined as

$$\Delta E_{mag} = E_{NM} - E_{FM} \quad (7)$$

yielding $\Delta E_{mag} = 0.06575$meV. Furthermore, the energy difference between the AFM and FM configurations,

$$\Delta E_{AFM-FM} = E_{AFM} - E_{FM} \approx -1.61 \text{ meV} \quad (8)$$

is extremely small, indicating a near degeneracy between these two magnetic states (Figure 24). Such a small exchange energy suggests weak magnetic coupling and implies that the magnetic ground state is only weakly sensitive to the relative spin alignment, with the dominant driving force being the overall energy lowering due to spin polarization [46-48].

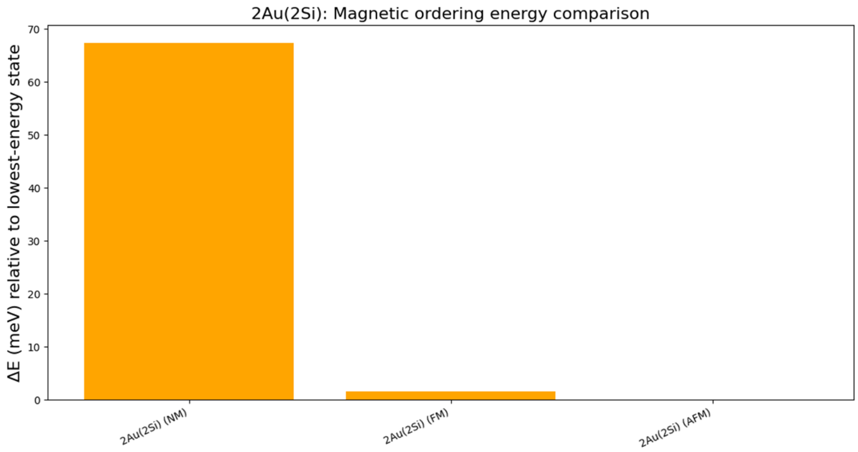

Figure 24. Relative energy differences (ΔE, meV) between NM, FM, and AFM states for the 2Au@2Si system, showing a small FM-AFM splitting (~1-2meV) indicative of near-degenerate magnetic orderings

The Curie temperature (T_C), which characterizes the thermal transition from a spin-polarized magnetic phase to a spin-degenerate paramagnetic state, was estimated using the mean-field approximation (MFA). This approach is widely adopted in first-principles studies of low-dimensional magnetic systems due to its conceptual simplicity and ability to provide qualitative trends in magnetic ordering temperatures [49, 50]. Within the MFA framework, the Curie temperature is directly related to the magnetic stabilization energy according to

$$k_B T_C^{MFA} \approx \frac{2}{3} \Delta E_{mag}. \quad (9)$$

Where k_B=8.617×10^{-5} eV/K is the Boltzmann constant and ΔE_{mag} represents the energy gain due to spin polarization. Using the calculated magnetic stabilization energy $\Delta E_{mag} = 0.06575$ eV for the 2Au@2Si configuration, the Curie temperature is estimated as

$$T_C^{MFA} = \frac{2}{3} \frac{0.06575}{8.617\times10^{-5}} \approx 5.1 \cdot 10^2 K.$$

Thus, the MFA-estimated Curie temperature of the Au-doped SiC nanosheet is approximately 510 K.

It should be emphasized that the present Curie temperature represents a mean-field approximation (MFA) estimate. The MFA neglects thermal spin fluctuations and spin-wave excitations, which are known to reduce the actual magnetic ordering temperature, particularly in low-dimensional and two-dimensional magnetic systems. Therefore, the calculated Tc value should be regarded as an approximate upper-limit estimate that reflects the tendency toward magnetic ordering rather than an exact prediction of the experimental Curie temperature.

The total-energy comparison for the five investigated configurations is summarized in Figure 23, which clearly shows that magnetic solutions for the same 2Au@2Si composition are energetically favored over the non-magnetic reference state. Furthermore, Figure 24 highlights the relative energy differences between the NM, FM, and AFM states for the 2Au@2Si system. The very small AFM–FM energy splitting (≈1-2 meV) indicates near degeneracy between different magnetic orderings, implying weak exchange interactions but a robust stabilization against the non-magnetic state.

A comparison of the estimated Curie temperature of the present Au-doped SiC nanosheet with previously reported transition-metal-doped SiC-based low-dimensional systems is provided in Table 12. Notably, the predicted T_C of approximately 510K exceeds those reported for V-, Fe-, and Mn-doped SiC nanostructures calculated using similar DFT-based MFA approaches [50]. This comparison highlights the effectiveness of Au substitution in stabilizing thermally robust magnetism in two-dimensional SiC systems.

Table 12. *Comparison of Curie temperatures of transition-metal–doped SiC-based low-dimensional systems calculated using DFT-based mean-field approximations, highlighting the highest estimated Curie temperature for the present Au-doped SiC nanosheet.*

System	Method	Tc (K)	Reference
V-doped SiC nanotube	DFT+U (MFA)	420	Physica E 158 (2024) 115641
Fe-doped SiC nanosheet	DFT+U (MFA)	460	Materials Science in Semiconductor Processing 197 (2025) 109702
Mn-doped SiC nanosheet	DFT (MFA)	380	Journal of Magnetism and Magnetic Materials *530* (2021) 167926
Au-doped SiC nanosheet (this work)	DFT+U (MFA)	≈ 510	Present work

The dependence of the Curie temperature on the magnetic stabilization energy is illustrated in Figure 25, which shows the linear relationship between T_C and ΔEmag within the MFA framework.

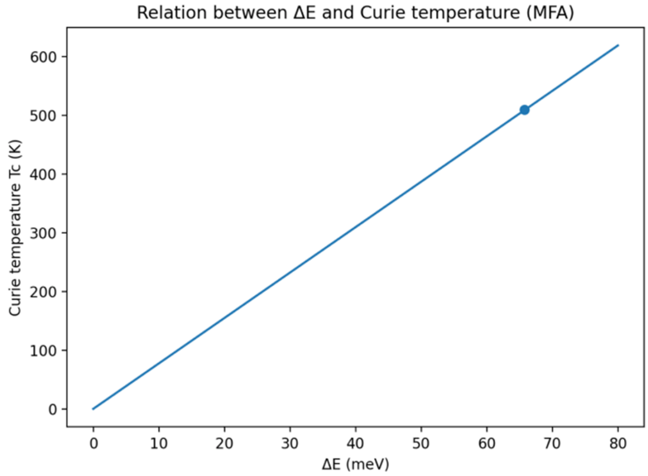

Figure 25. Mean-field-approximation (MFA) Curie temperature Tc as a function of the NM–FM energy difference ΔE, illustrating the estimated magnetic ordering temperature of the Au-doped SiC nanosheet.

The corresponding temperature dependence of the normalized magnetization is constructed using the standard mean-field expression

$$\frac{M(T)}{M_0} = \left(1 - \frac{T}{T_C}\right)^{1/2}, \qquad T < T_C, \tag{10}$$

as shown in Figure 26.

While pristine SiC and the non-magnetic reference configuration exhibit vanishing magnetization over the entire temperature range, the 2Au@2Si system retains a finite magnetization up to approximately T_C≈510K, confirming the thermal robustness of the dopant-induced magnetic state.

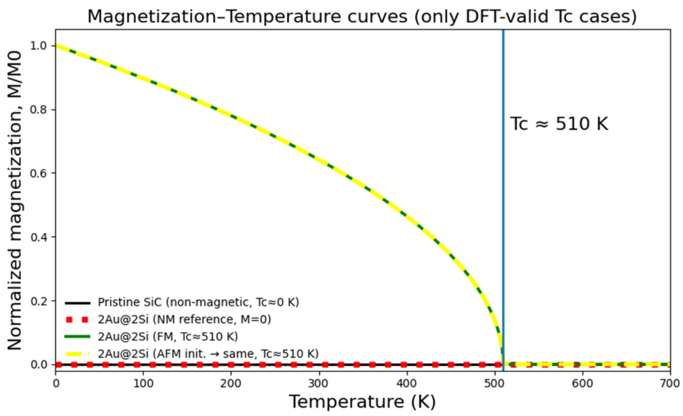

Figure 26. MFA-calculated normalized magnetization (M/M0) for 2Au@2Si, showing finite magnetization up to the estimated Tc ≈ 510 K within the mean-field approximation

Overall, the combined Mulliken spin population analysis, total-energy stability assessment, and MFA-based Curie temperature estimation consistently demonstrate that double Au substitution at Si sites stabilizes a robust high-temperature magnetic phase in SiC nanosheets. Importantly, the magnetism is predominantly mediated by dopant-induced electronic reconstruction within the carbon sublattice rather than by localized magnetic moments on the Au atoms themselves. The MFA-estimated Curie temperature suggests the possibility of magnetic ordering above room temperature. However, more sophisticated approaches beyond the mean-field approximation would be required to quantitatively predict the experimental Curie temperature.

4. CONCLUSIONS

In summary, a comprehensive spin-polarized first-principles investigation has been carried out to elucidate the electronic structure, magnetic behavior, and thermal stability of Au-doped two-dimensional SiC nanosheets. Single (1Au@Si) and double (2Au@2Si) substitutional doping configurations were systematically examined in a large supercell framework to minimize artificial dopant–dopant interactions and ensure a reliable assessment of intrinsic properties.

The results demonstrate that Au substitution provides an effective route for band-gap engineering in SiC nanosheets, leading to pronounced band-gap narrowing while preserving spin-degenerate band dispersions and the overall semiconducting character of the host material. Orbital-resolved density-of-states analysis reveals that the electronic reconstruction near the Fermi level is dominated by Au 5d states, with comparatively minor contributions from Au 6s and 6p orbitals.

Despite the absence of exchange splitting in the band structure, Mulliken spin population analysis uncovers robust dopant-induced magnetism mediated predominantly by the carbon sublattice. In the 1Au@Si configuration, a net magnetic moment of approximately 3 μB is stabilized, whereas double Au substitution gives rise to a ferrimagnetic-like ground state with a total magnetic moment of about 6 μB. Importantly, the magnetic solution is found to be insensitive to the initial spin configuration, as ferromagnetic and antiferromagnetic initializations converge to nearly identical magnetic states, highlighting the intrinsic and robust nature of the induced magnetism.

Total-energy comparisons confirm that spin-polarized states are energetically favored over the non-magnetic reference, with a very small energy difference between ferromagnetic and antiferromagnetic solutions. Mean-field estimation based on first-principles total-energy differences yields an estimated Curie temperature of approximately 510 K for the 2Au@2Si configuration. Since the mean-field approximation neglects thermal spin fluctuations, this value should be regarded as an approximate upper-limit estimate, suggesting the possibility of magnetic ordering above room temperature.

Overall, the present study establishes Au-doped SiC nanosheets as a promising class of two-dimensional dilute magnetic semiconductors in which band-gap tunability and the possibility of high-temperature magnetic ordering coexist.

The carbon-mediated nature of the induced magnetism, combined with the preservation of semiconducting behavior, highlights the strong potential of these systems for future spintronic and multifunctional nano-electronic applications.

Declarations

Ethics approval and consent to participate
Not applicable

Consent for publication
Not applicable.

Funding
This research did not receive any specific grant from funding agencies in the public, commercial, or not-for-profit sectors.

Acknowledgements
The authors gratefully acknowledge the computational resources and academic support provided by Azerbaijan State Oil and Industry University. The authors also acknowledge the Arifov Institute of Ion-Plasma and Laser Technologies (Uzbekistan) for institutional collaboration and scientific support.

Availability of data and materials
The datasets generated and analyzed during the current study are available from the corresponding author upon reasonable request.

Competing interests
The authors declare that they have no competing interests.

Authors' contributions
Sevda Rzayeva conceived and designed the study, performed the DFT simulations, analyzed the electronic and magnetic properties, and drafted the manuscript.
Yuldosh Yakubov contributed to the conceptual development, provided expertise on nanostructures, and reviewed the manuscript.
Umedjon Khalilov contributed to the scientific discussion, interpretation of the results, and critical revision of the manuscript.
All authors read and approved the final manuscript.

ORCID

Sevda Rzayeva, https://orcid.org/0009-0006-9747-3972; **Umedjon Khalilov,** https://orcid.org/0000-0003-3841-1895

REFERENCES

[1] A.K. Geim, and I.V. Grigorieva, "Van der Waals heterostructures," Nature, **499**, 419–425 (2013). https://doi.org/10.1038/nature12385
[2] S.A. Wolf, D.D. Awschalom, R.A. Buhrman, *et al*., "Spintronics: A spin-based electronics vision for the future," Science, **294**, 1488–1495 (2001). https://doi.org/10.1126/science.1065389
[3] D. Pesin, and A.H. MacDonald, "Spintronics and pseudospintronics in graphene and topological insulators," Nat. Mater. **11**, 409-416 (2012). https://doi.org/10.1038/nmat3305

[4] S. Chabi, and K. Kadel, "Two-Dimensional Silicon Carbide: Emerging Direct Band Gap Semiconductor," Nanomaterials, **10**, 2226 (2020). https://doi.org/10.3390/nano10112226
[5] R. Madar, "Materials science: silicon carbide in contention," Nature, **430**(7003), 974-975 (2004). https://doi.org/10.1038/430974a
[6] H. Ohno, Making nonmagnetic semiconductors ferromagnetic, Science **281**, 951–956 (1998). https://doi.org/10.1126/science.281.5379.951
[7] S. Sanvito, "Molecular spintronics," Chem. Soc. Rev. **40**, 3336-3355 (2011). https://doi.org/10.1039/c1cs15047b
[8] W. Chen, Q. Chen, J. Zhang, *et al*., "Electronic and magnetic properties of transition-metal-doped monolayer B_2S_2 within the GGA + U framework," RSC Adv. **14**, 3390–3399 (2024). https://doi.org/10.1039/D3RA08472H
[9] C. Gong, L. Li, Z. Li, *et al*., "Discovery of intrinsic ferromagnetism in two-dimensional van der Waals crystals," Nature, **546**, 265–269 (2017). https://doi.org/10.1038/nature22060
[10] V.N. Jafarova, S.S. Rzayeva, S. Popa, *et al*., Prediction of electronic, magnetic, and structural stability characteristics in Al- and Ga-doped single-walled SiC nanotubes: An ab initio study, Phys. Chem. Chem. Phys. **27**, 25980–26010 (2025). https://doi.org/10.1039/D5CP03523F
[11] S. Rzayeva, V.N. Jafarova, and D.D. Roy, "First-principles prediction of ferromagnetism and Curie temperature for transition-metal-doped (6,0) SiC nanotubes," Mater. Sci. Semicond. Process, **197**, 109702 (2025). https://doi.org/10.1016/j.mssp.2025.109702
[12] V.N. Jafarova, S.S. Rzayeva, V.I. Eminova, *et al*., "Theoretical investigation of electronic and magnetic characteristics of ZnSe substituted and co-substituted with transition metals," Int. J. Mod. Phys. B, **39**, 2550201 (2025). https://doi.org/10.1142/S0217979225502017
[13] V.N. Jafarova, S. S. Rzayeva, U. Abdurahmanova *et al*., "Spintronic potential of ZnSe doped with 3d transition metals: Insights from first-principles calculations," Indian J. Phys. (2025). https://doi.org/10.1007/s12648-025-03794-8
[14] M. Kurpas, P.E. Faria Junior, M. Gmitra, and J. Fabian, "Spin–orbit coupling in elemental two-dimensional materials," Phys. Rev. B, **100**, 125422 (2019). https://doi.org/10.1103/PhysRevB.100.125422
[15] J. He, G. Liu, C. Zhang, and G. Zhang, "Electronic structure and magnetic properties of noble metal (Rh, Ru, Pd, Ag) adsorbed vacancy-defective arsenene: A first-principles study," Int. J. Quantum Chem. **123**, e27197 (2023). https://doi.org/10.1002/qua.27197
[16] Q.J. Wang, Q.H. Tan, and Y.K. Liu, "Magnetic properties in carbon-doped In2O3: A density functional theory investigation," Physica B: Condensed Matter, **450**, 54–57 (2014). https://doi.org/10.1016/j.physb.2014.05.033
[17] S. Smidstrup, T. Markussen, P. Vancraeyveld, *et al*., "QuantumATK: An integrated platform of electronic and atomic-scale modelling tools, J. Phys.: Condens. Matter, **32**, (2020) 015901. https://doi.org/10.1088/1361-648X/ab4007
[18] O. Gunnarsson, and B.I. Lundqvist, "Exchange and correlation in atoms, molecules, and solids by the spin-density-functional formalism," Phys. Rev. B, **13**, 4274–4298 (1976). https://doi.org/10.1103/PhysRevB.13.4274
[19] J. P. Perdew, and A. Zunger, "Self-interaction correction to density-functional approximations for many-electron systems," Phys. Rev. B, **23**, 5048–5079 (1981). https://doi.org/10.1103/PhysRevB.23.5048
[20] J. Junquera, Ó. Paz, D. Sánchez-Portal, and E. Artacho, "Numerical atomic orbitals for density functional calculations," Phys. Rev. B, **64**, 235111 (2001). https://doi.org/10.1103/PhysRevB.64.235111
[21] G. Kresse, and J. Furthmüller, "Efficient iterative schemes for ab initio total-energy calculations using a plane-wave basis set," Phys. Rev. B, **54**, 11169–11186 (1996). https://doi.org/10.1103/PhysRevB.54.11169
[22] Y. Ding, Y. Wang, J. Ni, *et al*., "First principles study of structural, elastic, and electronic properties of graphene-like MX_2 (M = Si, Ge; X = C, Si)," Physica B: Condensed Matter, **406**, 2254–2260 (2011). https://doi.org/10.1016/j.physb.2011.03.012
[23] H. Zhang, Y. Ma, and Z. Chen, "Stability and electronic properties of two-dimensional silicon carbide sheets," Solid State Commun. **151**, 1641–1645 (2011). https://doi.org/10.1016/j.ssc.2011.08.028
[24] H. Sahin, S. Cahangirov, M. Topsakal, and S. Ciraci, "Monolayer honeycomb structures of group-IV elements and III–V binary compounds," Phys. Rev. B, **80**, 155453 (2009). https://doi.org/10.1103/PhysRevB.80.155453
[25] K. Dolui, I. Rungger, and S. Sanvito, "Origin of the doping asymmetry in two-dimensional materials," Phys. Rev. B, **87**, 165402 (2013). https://doi.org/10.1103/PhysRevB.87.165402
[26] X. Yang, Y. Shen, J. Liu, X. Meng, X. Gao, L. Lv, M. Zhou, Y. Zhang, Y. Zheng, and Z. Zhou, "Electronic and optical properties of a novel two-dimensional semiconductor material $TlPt_2S_3$: A first-principles study," Phys. Chem. Chem. Phys. 24, 7642–7652 (2022). https://doi.org/10.1039/D1CP05918A
[27] Z. Zhang, X. Liu, J. Yu, *et al*., "Tunable electronic and magnetic properties of two-dimensional materials and their one-declensional derivatives," WIREs Comput. Mol. Sci. **6**, e1251 (2016). https://doi.org/10.1002/wcms.1251
[28] Y. Li, Z. Zhou, S. Zhang, and Z. Chen, "MoS_2 nanoribbons: high stability and unusual electronic and magnetic properties," J. Am. Chem. Soc. **130**, 16739–16744 (2008). https://doi.org/10.1021/ja805545x
[29] V.N. Jafarova and S. Rzayeva, "The effect of doping on the electronic and magnetic properties of GaN nanotubes: A preliminary study within the framework of LDA and LDA+U methods," Journal of the Faculty of Engineering and Architecture of Gazi University, **40** (4), 2627–2634 (2025). https://doi.org/10.17341/gazimmfd.1625213
[30] R.S. Mulliken, "Electronic population analysis on LCAO–MO molecular wave functions. I," J. Chem. Phys. **23**, 1833–1840 (1955). https://doi.org/10.1063/1.1740588
[31] J.P. Perdew, K. Burke, and M. Ernzerhof, "Generalized gradient approximation made simple," Phys. Rev. Lett. **77**, 3865–3868 (1996). https://doi.org/10.1103/PhysRevLett.77.3865
[32] S. Chabi, and K. Kadel, "Two-dimensional Silicon carbide: emerging direct band gap semiconductor," Nanomaterials, **10**, 2226 (2020). https://doi.org/10.3390/nano10112226
[33] S. Chabi, Z. Guler, A. Brearley, *et al*., "The creation of true two-dimensional silicon carbide," Nanomaterials, **11**, 1799 (2021). https://doi.org/10.3390/nano11071799
[34] Z. Shi, Z. Zhang, A. Kutana, and B.I. Yakobson, "Predicting two-dimensional silicon carbide monolayers," ACS Nano, **9**, 9802-9809 (2015). https://doi.org/10.1021/acsnano.5b02753

[35] R. Katoch, and S. Jain, "Magnetic Properties of 2D Materials," in: *Emerging Two Dimensional Materials and Applications*, (CRC Press, 2022), pp. 95–122. https://doi.org/10.1201/9781003247890-6
[36] M. Luo, Y.H. Shen, and T.L. Yin, "Ab initio study of electronic and magnetic properties in TM-doped SiC, Physica E: Low-dimensional Systems and Nanostructures," **85**, 280–284 (2017). https://doi.org/10.1016/j.physe.2016.08.028
[37] L. Jiang, Y. Dong and Z. Cui, "Adsorption of metal atoms (including Au) on SiC monolayer: electronic and magnetic properties from DFT," Inorganics, **11**, 240 (2023). https://doi.org/10.3390/inorganics11060240
[38] L. Zhang, and Z. Cui, "First-Principles Study of Metal Impurities in Silicon Carbide: Structural, Magnetic, and Electronic Properties," Front. Mater. **9**, 956675 (2022). https://doi.org/10.3389/fmats.2022.956675
[39] O.V. Yazyev, and L. Helm, "Defect-induced magnetism in graphene," Phys. Rev. B, **75**, 125408 (2007). https://doi.org/10.1103/PhysRevB.75.125408
[40] R.R. Nair, I.-L. Tsai, M. Sepioni, *et al*., "Dual origin of defect magnetism in graphene and its reversible switching by doping," Nat. Commun. **4**, 2010 (2013). https://doi.org/10.1038/ncomms3010
[41] J. Hernández-Tecorralco, L. Meza-Montes, M. E. Cifuentes-Quintal, *et al*., "Understanding the sp magnetizm in substitutionally doped graphene: a first-principles study," Phys. Rev. B, **105**, 224425 (2022). https://doi.org/10.1103/PhysRevB.105.224425
[42] M. Houmad, O. Dakir, H. Benzidi, *et al*., "Magnetic behavior of Mn-doped SiC nanosheet," Int. J. Mod. Phys. B, **31**, 1750163 (2017). https://doi.org/10.1142/S0217979217501636
[43] X. He, T. He, Z. Wang, and M. Zhao, "Neutral vacancy-defect-induced magnetism in SiC mono-layer," Physica E, **42**, 2451-2454 (2010). https://doi.org/10.1016/j.physe.2010.06.010
[44] Q. Wei, Y. Yang, G. Yang, and X. Peng, "New stable two-dimensional silicon carbide nanosheets," J. Alloys Compd. **868**, 159201 (2021). https://doi.org/10.1016/j.jallcom.2021.159201, arXiv: arXiv.2012.07841
[45] J. Hafner, "Ab-initio simulations of materials using VASP: Density-Functional theory and Beyond," J. Comput. Chem. **29**, 2044-2078 (2008). https://doi.org/10.1002/jcc.21057
[46] M. Pajda, J. Kudrnovský, I. Turek, *et al.*, "Ab initio calculations of exchange interactions, spin-wave stiffness, and Curie temperatures of Fe, Co, and Ni," Phys. Rev. B, **64**, 174402 (2001). https://doi.org/10.1103/PhysRevB.64.174402
[47] S. Rusz, L. Bergqvist, J. Kudrnovský, and I. Turek, "Exchange interactions and Curie temperatures of diluted magnetic systems," Phys. Rev. B, **73**, 214412 (2006). https://doi.org/10.1103/PhysRevB.73.214412
[48] K. Sato, L. Bergqvist, J. Kudrnovský, *et al*., "First-principles theory of dilute magnetic semiconductors," Rev. Mod. Phys. **82**, 1633–1690 (2010). https://doi.org/10.1103/RevModPhys.82.1633
[49] M. Pajda, J. Kudrnovský, I. Turek, *et al*., "Ab initio calculations of exchange interactions, spin-wave stiffness constants and Curie temperatures of Fe, Co and Ni," Phys. Rev. B, **64**, 174402 (2001). https://doi.org/10.1103/PhysRevB.64.174402
[50] S. Rusz, L. Bergqvist, J. Kudrnovský, and I. Turek, "Exchange interactions and Curie temperatures in $Ni_{2-x}MnSb$ alloys: First-principles study," Phys. Rev. B, **73**, 214412 (2006). https://doi.org/10.1103/PhysRevB.73.214412

ЗОЛОТО-ІНДУКОВАНИЙ МАГНЕТИЗМ ТА ТЕРМІЧНА СТАБІЛЬНІСТЬ У НАНОЛИСТАХ SiC: DFT+U

Севда Рзаєва[1], Юлдош Якубов[2], Умеджон Халілов[3,4,5], Мафтун Алієв[6], Аріель Шарон Асаре[7,8]
[1]*Азербайджанський державний університет нафти та промисловості, проспект Азадлиг, 20, AZ-1010, Баку, Азербайджан*
[2]*Інститут загальної та неорганічної хімії, Мірзо-Улугбек 77-а, 100170 Ташкент, Узбекистан*
[3]*Інститут іонно-плазмових та лазерних технологій ім. Аріфова, Дурмон юлі 33, 100120 Ташкент, Узбекистан*
[4]*Антверпенський університет, Грюненборгерлан 171, Антверпен 2020, Бельгія*
[5]*Інженерна школа, Центральноазіатський університет, Ташкент 111221, Узбекистан*
[6]*Нахчиванський державний університет, Нахчивань, Азербайджан*
[7]*Кафедра фізики, Університет Гани*
[8]*Міжнародний центр теоретичної фізики імені Абдуса Салама (ICTP), Італія*

Двовимірні нанолисти карбіду кремнію (SiC), леговані золотом, досліджуються за допомогою теорії спін-поляризованої густини (DFT+U) для вивчення їхньої електронної структури, індукованого магнетизму та термічної стабільності. Одинарні (1Au@Si) та подвійні (2Au@2Si) конфігурації заміщення моделюються в суперкомірці 4×4 для забезпечення надійної оцінки власних властивостей. Включення Au значно звужує ширину забороненої зони, зберігаючи при цьому напівпровідниковий характер нанолиста SiC. Аналіз густини станів зі спіновим розрізненням показує, що 5d-орбіталі Au домінують в електронних станах поблизу рівня Фермі. Незважаючи на майже спін-вироджені дисперсії зон, аналіз спінової популяції Маллікена виявляє індукований легуючими речовинами магнетизм, опосередкований сусідніми атомами вуглецю. Система 1Au@Si демонструє магнітний момент ~3 μB, тоді як конфігурація 2Au@2Si стабілізує феримагнітний стан із загальним магнітним моментом ~6 μB. У наближенні середнього поля оцінена температура Кюрі становить приблизно 510 K, що свідчить про можливість магнітної стабільності вище кімнатної температури та потенційне застосування в спінтронічних пристроях.
Ключові слова: *нанолисти SiC; легування золотом; спінтроніка; розбавлені магнітні напівпровідники; теорія функціоналу густини; температура Кюрі*